21st Australasian Fluid Mechanics Conference
Adelaide, Australia
10-13 December 2018

Modelling of a Cantilevered Flexible Plate undergoing Large-Amplitude Oscillations due to a High Reynolds-Number Axial Flow.

R. O. G. Evetts, R. M. Howell and A. D. Lucey

Fluid Dynamics Research Group, Department of Mechanical Engineering,
Curtin University of Technology, GPO Box U1987, Perth, Western Australia 6845

Abstract

We present development of a model of the non-linear fluid-structure interaction of a cantilevered flexible plate with an ideal flow that can account for the effect of boundary-layer separation from the plate surface upstream of its trailing edge. The model also allows for the wake to be formed solely from the trailing edge, an assumption used in previous studies of the system that also constrain the path of its lumped vorticity thereby precluding roll-up. Short plates are studied herein for which the behaviour is dominated by low-order structural modes. When the wake is forced to form from the trailing edge the typical sequence of amplitude growth to non-linearly saturated oscillations at flow speeds above that of the onset of linear instability is found. However, if separation is included the system evidences the same sequence at a flow speed for which the system is neutrally stable to linear disturbances. This suggests that flow separation may be the cause of the sub-critical instability found in experimental studies of the system. The mechanism for this effect is briefly discussed though a consideration of the wake dynamics. The reduced complexity of our model relative to others allows us then to offer further insights into the origins of the sub-critical instability.

Introduction

Extending our work of [4] we further develop our model of the non-linear fluid-structure interaction (FSI) of a cantilevered flexible plate of length L in uniform axial flow of velocity U_∞ as depicted in figure 1. Inviscid flow is assumed and therefore the FSI model approximates the very high Reynolds number (Re) flows that predominate in engineering applications. However, viscous effects are implicitly incorporated either through the imposition of the Kutta condition at the plate's trailing edge or through boundary-layer separation (as drawn in figure 1) that can occur in an adverse pressure gradient upstream of the trailing edge. Previous approaches, for example [11, 12], have modelled this FSI system using the former whereby the wake forms from the trailing edge and in [12] is assumed to follow a sinusoidal path following the spatio-temporal characteristics of the plate motion. Therefore, the main purpose of this paper is to determine the effect of flow separation on the non-linear stability of the FSI system by comparing its results with those in which the boundary-layer vorticity is assumed to remain attached on both sides for the full length of the flexible plate.

The latest experiments on this FSI are provided by [14], who also present a comparison of their results with those of the model presented in [12] which showed excellent agreement for the limit of linear stability. However, the theoretical model predicted a supercritical bifurcation while their experiment demonstrated a subcritical bifurcation creating a *hysteresis loop*. With regards to the origin of hysteresis in this FSI, they reiterated the explanation posed in [3, 12]: that large aspect ratio plates suffer more from spanwise deformations which have a psuedo-stiffening effect leading to higher critical velocities.

As yet numerical modelling has been unable to capture the hysteresis phenomenon because modelling is still restricted to values of Re that are too low for separation to occur. Furthermore, the type of model employed is usually very complex *e.g.* direct-numerical simulation, leading to difficulty in exploring the underlying physics with regards to the specific interactions involved in the hysteresis phenomenon. The most complete numerical study to date of a flag in viscous flow is provided by [2] reaching $Re = 10^3$. They coupled a finite-element model to a solver for thin membrane dynamics of arbitrarily large motion. They identified three distinct regimes of instability: (I) fixed-point stability, in which the flag settles into a stable non-oscillatory straight form; (II) limit-cycle flapping, where the body enters steady oscillations of constant amplitude and frequency; and (III) chaotic flapping, where the flag undergoes irregular non-periodic flutter.

Herein it is shown that the simple high-Re model developed is able to capture hysteresis and that the reduced complexity of our model relative to others allows us to more deeply investigate its origins.

Method

The present solution of the Laplace equation utilises a non-linear boundary-element flow solution similar to that developed in [7] and is an extension of the second-order linear boundary-element method detailed in [5] so as to capture finite-amplitude effects. The flexible plate is discretised into N panels each of length $\delta s = L/N$ and the vector of non-linear vortex strengths, γ, for the N panels is found by imposing the no-flux condition giving

$$\{\gamma\} = [\mathbf{I^N}]^{-1}\{U_\infty \sin\theta + \dot{\eta}\cos\theta - \dot{x}\sin\theta + u^{Tb}\sin\theta - u^{Nb}\cos\theta\}, \quad (1)$$

where θ is the panel angle relative to $y = 0$ and $\dot{x}$ and $\dot{\eta}$ are respectively the velocities of each panel control point in the x- and y-directions. u^{Nb} and u^{Tb} are respectively the normal and tangential velocities induced at the panel control points by the discrete vortices of the wake. $[\mathbf{I^N}]$ comprises the normal influence coefficients. The non-linear version of the Euler-Bernoulli

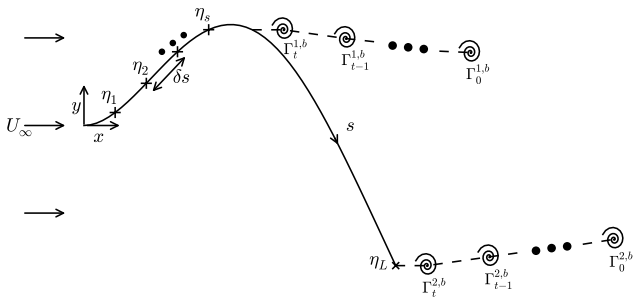

Figure 1: Schematic of the fluid-structure system studied and the approach taken to model separation.

beam equation, presented in [9, 11], is

$$\delta p = \rho h \ddot{\eta}_s - \rho h \frac{\partial \eta}{\partial s} \int_0^s \left(\left(\frac{\partial^2 \eta}{\partial t \partial s} \right)^2 + \frac{\partial \eta}{\partial s} \frac{\partial^3 \eta}{\partial t^2 \partial s} \right) \mathrm{d}s - \rho h \frac{\partial^2 \eta}{\partial s^2} \int_s^L \int_0^s \left(\left(\frac{\partial^2 \eta}{\partial t \partial s} \right)^2 + \frac{\partial \eta}{\partial s} \frac{\partial^3 \eta}{\partial t^2 \partial s} \right) \mathrm{d}s\mathrm{d}s + B \left[\frac{\partial^4 \eta}{\partial s^4} + \frac{\partial^4 \eta}{\partial s^4} \left(\frac{\partial \eta}{\partial s} \right)^2 + 4 \frac{\partial \eta}{\partial s} \frac{\partial^2 \eta}{\partial s^2} \frac{\partial^3 \eta}{\partial s^3} + \left(\frac{\partial^2 \eta}{\partial s^2} \right)^3 \right], \quad (2)$$

where ρ, h, and B are the plate density, thickness, and stiffness respectively. This model is based upon the assumption that the plate is inextensible; thus, L and therefore δs are constant. To determine the pressure difference across the plate, δp, the vortex-singularity strengths found from equation 1 are used to determine the flow perturbations (from the mean flow) and the velocity potential. These are then used in the unsteady Bernoulli pressure equation (see [5]) applied along the upper and lower surfaces of the flexible plate. When separation occurs, the surface pressure downstream of the separation point is taken to be that at the point of separation.

We decompose the transmural pressure using $\delta p = \delta p' + \rho_f [\mathbf{B}] \ddot{\eta}$ to separate out the fluid inertia; herein ρ_f is the fluid density and $[\mathbf{B}]$ is a matrix that contains the influence coefficients of the velocity potential. Combining this with equation 2 gives an equation for the coupled fluid-structure system. This is rearranged for plate acceleration and is solved using a semi-implicit Crank-Nicholson-type method of solution, detailed in [8], that solves first for the plate acceleration at the next time step followed by integration to determine velocities and displacements. The wake formed by the separation of vorticity from the plate is modelled using a non-linear version of the discrete-vortex method described in [5] by Gaussian blobs of strength Γ shown in figure 1.

The model without separation was validated by comparison with [12], see figure 2, whose results are shown in the left hand column of figure. The corresponding results from the current model are shown in the right hand column. The first two rows of figures show the evolution of the vertical and horizontal tip deflection in time. The third row of figures shows snapshots of the plate at a number of time steps through the simulation. The fourth and fifth row of figures show the phase plots of the plate tip in the x- and y-directions respectively, and the final row shows a plot of the tip deflection in the x- and y-directions. It can be seen that in each row there is good agreement between the two models, each case achieving similar scale deflections and shapes once the plate deflection has saturated and the limit cycle behaviour has been reached. It should be noted that there are two key difference between the model presented in [12] and the current model. Firstly, in the current model the wake is allowed to move freely, whereas the wake used by [12] is assumed to travel along a sinusoidal path. Secondly, the model presented by [12] employs the Galerkin method and takes account of the first 6 modes, while the current model supports any number of modal shapes that may arise.

Separation was chosen to occur downstream of the point where an adverse pressure gradient was detected on either the upper or lower surface of the plate when it exceeds a percentage threshold pressure value P_{th} of the dynamic pressure $\rho_f U_\infty^2$. It is stated in the literature, *e.g.* [6], that it is impossible to predict the separation point accurately without some *a priori* knowledge from experiments. Thus it is not known what the exact value of threshold pressure for separation should be for the full FSI studies, though our model can be calibrated against available experimental results, *e.g.* [3, 10]. However, the rigid-body separation model can be more thoroughly validated: this was done by applying the model to two different NACA aerofoils and the

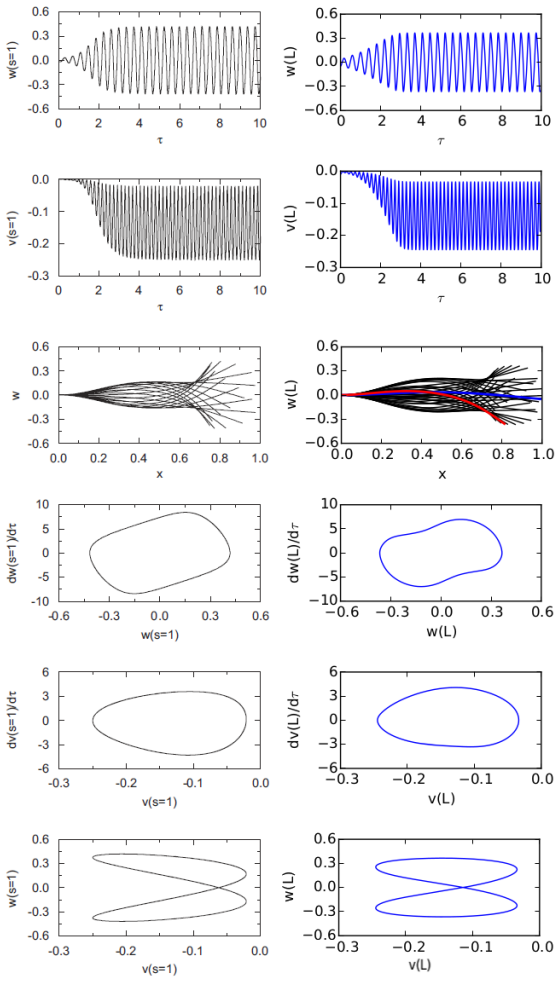

Figure 2: A comparison between the full numerical model (right) with no shear-layer separation, and the results presented by [12] (left).

results were compared to the exhaustive experimental results of [1]. When the model was applied to a symmetric aerofoil and it predicted separation to occur at incidence $\alpha \approx \pm 22^{\text{o}}$ while in the experimental results it was $\approx \pm 15^{\text{o}}$. When the model was applied to a cambered aerofoil, the predicted separation point (16^{o}) was much closer to the experimental result (14^{o}). There are a number of potential reasons for differences between our theoretical model and the experimental results *e.g.* there are other viscous effects that affect the result such as wall effects and blockage, which do not arise in the model presented. Following this validation, it was adjudged that when applied to the flexible plate, separation from the plate surface would occur at $P_{\text{th}} = 0.05$.

Results

Results are presented in terms of non-dimensional time $\bar{T} = T\rho_f^2 B^{1/2}/(\rho h)^{5/2}$, flow speed $\bar{U} = U_\infty (\rho h)^{3/2}/(\rho_f B^{1/2})$ and fluid-to-plate mass ratio $\bar{L} = \rho_f L/(\rho h)$ following the scheme presented in [5]. Herein, we use $\bar{L} = 1$ throughout that broadly corresponds to the short plates for which the FSI dynamics are dominated by low-order flexible-plate modes [5, 11, 12].

We showed in [4] that when the effect of separation upstream of the trailing edge was included at flow speeds much greater than U_c, it was found that the effect on system behaviour was negligible. However, also shown in [4], at lower flow speeds

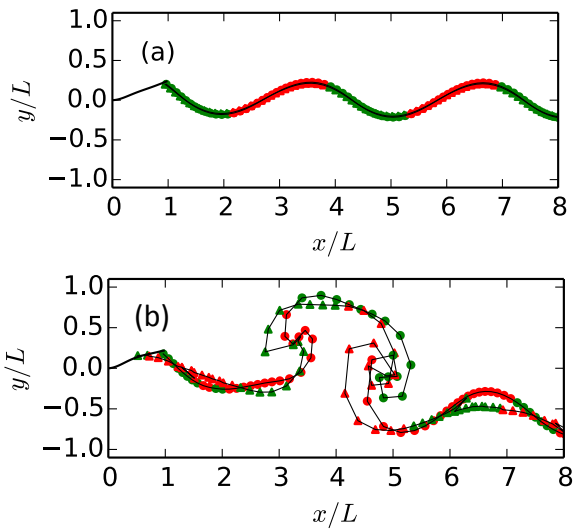

Figure 3: Wake vorticity generated by a plate undergoing non-linear oscillations for $\bar{L} = 1$ with $\bar{U} = 5.50$: (a) wake vorticity is forced to separate at the trailing edge; (b) separation is modelled. Markers denote a wake vortex shed from either the trailing edge (•), or the separation point (△). Colour denotes vorticity polarity: green - positive, red - negative.

wake-separation effects are found to be very significant. In the absence of separation, after applying the initiating finite-amplitude deflection the plate motion settles quickly into low-amplitude neutrally-stable oscillations as predicted by linear studies. By contrast, amplitude growth followed by non-linear saturation when the plate settles in to limit-cycle oscillations are observed when separation is included in the model. This demonstrates that flow separation can cause non-linear instability at a flow speed for which the system is linearly stable. This type of non-linear sub-critical instability, that causes hysteresis as flow speed is changed, is well known in experimental studies of cantilevered flexible-plate/flag flutter.

To understand the effect of separation on non-linear motions and stability of the flexible plate, figure 3 shows the wake structures at $\bar{U} = 5.50$ when the flow is (a) forced to remain attached for the full length of the plate and (b) when separation is modelled. First, (a) demonstrates that the assumption, e.g. in the models of [12], that wake vortices follow a sinusoidal path when separation occurs at the trailing edge is valid. Second, the effect of separation on stability, discussed above, can be deduced from the structure of the wake in (b). At high flow speed, it was observed that intense vortical structures form but that these convect downstream rapidly and have little effect on the plate behaviour. In contrast, for lower flow speeds, roll-up occurs much closer to the trailing edge of the plate (located at $x/L = 1$ in these figures) and these structures can therefore exercise a significant effect on the flow field that drives the plate motion.

The effect of separation was examined over a range of flow speeds and at a number of values of P_{th}. Initial results (not shown) for $\bar{U}$ = 7.16 (approximately 40% above the critical velocity for the linear model) were carried out for P_{th} = 0.001, 0.01, 0.1 and 10, the last found to be high enough to prohibit flow separation upstream of the trailing edge entirely. Decreasing the P_{th} from 10 downwards, the system was unaffected until $P_{\text{th}} = 0.01$ when the system began to take longer to reach saturation and was much less stable. It was found that separation occurred at approximately 40% of the time steps using this pressure threshold value. These effects were seen to increase as P_{th} was further decreased until finally $P_{\text{th}} = 0$ where the beam was unable to maintain self-sustaining oscillations.

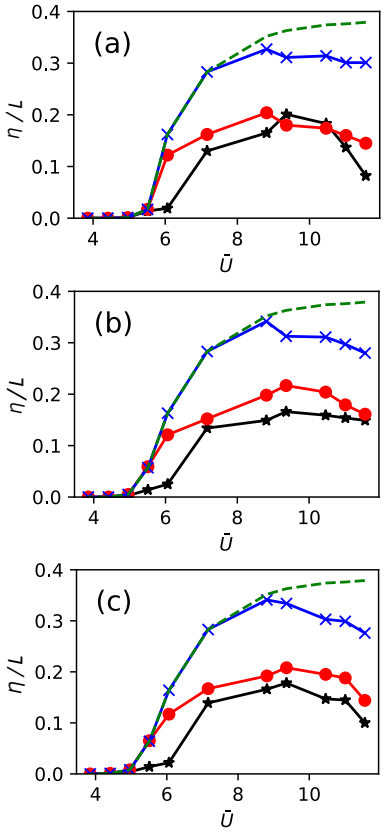

Figure 4: The deflection predicted for $\eta_L^{t=0}$ (a) $0.01L$, (b) $0.1L$, and (c) $0.2L$. P_{th}: 0.001 (⋆), 0.01 (•), 0.1 (×), 10.0 (−−).

Figure 4 shows the results gained using these same pressure thresholds over a range of flow speeds and using different initial deflections. Figure 4(a), (b), and (c) show the results for $\eta_L^{t=0} = 0.01$, 0.1, and 0.2 respectively, the value in (a) representing the results when the initial deflection is close to the linear regime. It is seen that as the flow speed increases, each case has the same critical velocity, though for larger initial deflections; in Figures 4(b) and (c), the amplitude of the oscillations at these lower flow speeds is greater than in Figure 4(a). At each initial deflection the line of P_{th} = 0.1 is identical to the P_{th} = 10 result until $\bar{U} \approx 7$, above which the results begin to diverge slightly as flow separation upstream of the trailing edge begins to occur as the combination of flow speed and amplitude are enough to overcome the threshold pressure. For the lower threshold pressures it is seen that this point is reached much sooner. In all cases each curve displays a consistent drop in steady-state amplitude above a certain flow speed. This is a result of the increasing levels of separation that were observed with increasing flow speed. For example it was seen during the experiments that for P_{th} = 0.1 at $\bar{U} = 8.81$ and $\eta_L^{t=0} = 0.2$ that the flow would separate in approximately 10% of the time steps, however at $\bar{U} = 11.5$ separation occurred at 50% of the time steps.

From the above results it is clear that separation upstream of the trailing edge has a significant effect on the system, causing the system to take longer to reach saturation, and lowering the oscillation amplitude achieved. It can also be seen that the final results predicted by each model are mostly independent of the initial deflection, the only notable exception being at flow speeds close to the critical velocity, where bi-stability can be observed.

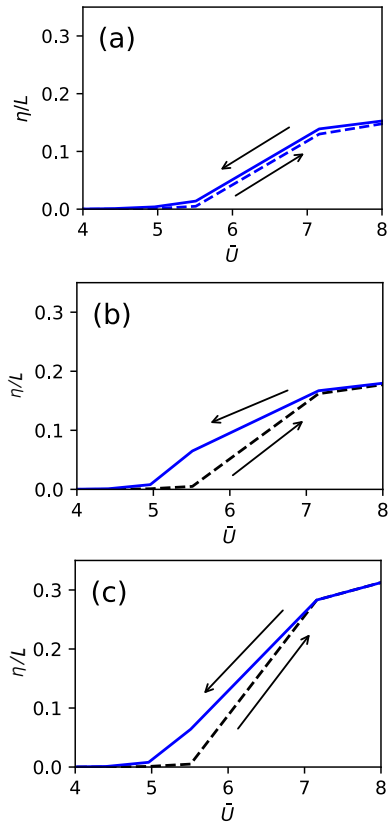

Figure 5: Hysteresis loops at $\bar{L} = 1$: The maximum stable deflection achieved when first increasing and then decreasing the flow speed for P_{th} values of (a) 0.001, (b) 0.01, and (c) 0.1. In each case the dashed and solid lines represent the deflection achieved when increasing and decreasing the flow speed respectively.

To allow the model to more closely mimic the continuous transition between flow speeds seen in physical experiments, the final state of the model at one flow speed was used as the initial conditions for the next. The results produced by this pseudo-continuous model are shown in figure 5(a)-(c) using values of P_{th} of (a) 0.001, (b) 0.01, and (c) 0.1. The dashed line shows the amplitude of the oscillations when the flow speed is increased, while the solid line shows the same amplitude when the flow speed is decreased. It can be seen that for $P_{\text{th}} = 0.001$ no hysteresis loop is observed. However, for $P_{\text{th}} = 0.01$ and 0.1 a clear sub-critical hysteresis loop is seen, where the system is able to maintain self-sustaining oscillations below the critical velocity. In each case the size of hysteresis loop is similar, the system becoming unstable initially at $\bar{U} = 5.51$, and returning to stability at $\bar{U} = 4.95$. The sizes of the hysteresis loops found are much smaller than those found in the experimental results of [13] However, the flow speeds over which hysteresis is observed are similar, as are the amplitudes of the oscillations.

Conclusions

We have developed a computational model to simulate non-linear oscillations of a cantilevered plate in potential flow that can incorporate the effects of boundary-layer separation upstream of the trailing edge that would occur in regions of high adverse pressure gradient along the plate. The main new findings of the present study arise from the effects of separation. At flow speeds much higher than the critical speed for linear instability, the effects of separation are not significant. Amplification and subsequent non-linear saturation at finite amplitudes can be adequately modelled by wake formation from the trailing edge of the plate as has been done in previous studies. However, at lower flow speeds separation is destabilising. In particular, at the flow speed for which the system is neutrally stable to linear disturbances, we have shown that separation can lead to non-linear instability and ensuing limit-cycle flutter. This suggests that flow separation may be a mechanism for the sub-critical instability that is observed in experimental work. The reduced complexity of our model relative to others then allowed us to further investigate the origins of the hysteresis instability. It was shown that a critical value of P_{th} exists for hysteresis to occur and that its intensity can be varied by varying the magnitude of P_{th}. Also non-linear instability with separation was mostly independent of initial plate amplitude. Future work will continue to investigate further the origins of the hysteresis phenomenon.

References

[1] Abbott, I. H. and von Doenhoff, A. E., *Theory of Wing Sections*, Dover Publications Inc, 1959, first edition.

[2] Connell, B. S. H. and Yue, D. K., Flapping dynamics of a flag in a uniform stream, *Journal of Fluid Mechanics*, **581**, 2007, 33–67.

[3] Eloy, C., Lagrange, R., Souilliez, C. and Schouveiler, L., Aeroelastic instability of cantilevered flexible plates in uniform flow, *Journal of Fluid Mechanics*, **611**, 2008, 97–106.

[4] Evetts, R. O. G., Howell, R. M. and Lucey, A. D., Modelling of a cantilevered flexible plate undergoing large-amplitude oscillations due to a high reynolds-number axial flow, in *Proceedings of the 3rd Symposium on Fluid-Structure-Sound Interactions and Control*, Germany: Springer-Verlag, 2016, 339-344.

[5] Howell, R. M., Lucey, A. D., Carpenter, P. W. and Pitman, M. W., Interaction between a cantilevered-free flexible plate and ideal flow, *Journal of Fluids and Structures*, **25**, 2009, 544–566.

[6] Katz, J. and Plotkin, A., *Low-Speed Aerodynamics*, Cambridge University Press, 2010, second edition.

[7] Lucey, A. D., Cafolla, G. J., Carpenter, P. W. and Yang, M., The non-linear hydroelastic behaviour of flexible walls, *Journal of Fluids and Structures*, **11**, 1997, 717–744.

[8] Lucey, A. D. and Carpenter, P. W., A numerical simulation of the interaction of a compliant wall and inviscid flow, *Journal of Fluid Mechanics*, **234**, 1992, 121–146.

[9] Moretti, P. M., Tension on fluttering flags, *Journal of Acoustics and Vibration*, **8**, 2003, 227–230.

[10] Shelley, M., Vandenberghe, N. and Zhang, J., Heavy flags undergo spontaneous oscillations in flowing water, *Physical Review Letters*, **94**.

[11] Tang, D. M. and Dowell, E. H., Limit cycle oscillations of two-dimensional panels in low subsonic flow, *International Journal of Non-Linear Mechanics*, **37**, 2002, 1199–1209.

[12] Tang, L. and Païdoussis, M. P., On the instability and the post-critical behaviour of two-dimensional cantilevered flexible plates in axial flow, *Journal of Sound and Vibration*, **305**, 2007, 97–115.

[13] Watanabe, Y., Suzuki, S., Sugihara, M. and Sueoka, Y., An experimental study of paper flutter, *Journal of Fluids and Structures*, **16**, 2002a, 529–542.

[14] Zhao, W., Païdoussis, M. P., Tang, L., Liu, M. and Jiang, J., Theoretical and experimental investigations of the dynamics of cantilevered flexible plates subjected to axial flow, *Journal of Sound and Vibration*, **331**, 2012, 575–587.